Microporous and Mesoporous Materials 151 (2012) 411–417

Contents lists available at SciVerse ScienceDirect

Microporous and Mesoporous Materials

journal homepage: www.elsevier.com/locate/micromeso

Mercaptopropyl-functionalized helical mesoporous silica nanoparticles with *c2mm* symmetry: Cocondensation synthesis and structural transformation in the dilute solution of mixed cationic and nonionic surfactants

Wei-Chia Huang [a], Nien-Chu Lai [a], Li-Ling Chang [a], Chia-Min Yang [a,b,*]

[a] Department of Chemistry, National Tsing Hua University, Hsinchu 30013, Taiwan
[b] Frontier Research Center on Fundamental and Applied Sciences of Matters, National Tsing Hua University, Hsinchu 30013, Taiwan

ARTICLE INFO

Article history:
Received 27 August 2011
Received in revised form 23 September 2011
Accepted 23 September 2011
Available online 12 October 2011

Keywords:
Helical mesoporous silica
Mercaptopropyl functionalization
c2mm symmetry
Cocondensation
Structural transformation

ABSTRACT

Mercaptopropyl-functionalized mesoporous silica nanoparticles with *c2mm* symmetry and short-pitch helical channels were prepared by the cocondensation synthesis in the dilute solution of cetyltrimethylammonium bromide and tetraethylene glycol dodecyl ether ($C_{12}EO_4$) under alkaline conditions. The amount and distribution of the covalently coupled organic groups within the nanoparticles were investigated. Interestingly, the mesostructure transformed toward *p6mm* phase when the amount of mercaptopropyltrimethoxysilane was increased, and a reverse *p6mm*-to-*c2mm* transformation took place as the mole percentage of $C_{12}EO_4$ was further increased. The presence of $C_{12}EO_4$ was also found crucial for helical arrangement of the channels. *In situ* small-angle X-ray scattering measurements showed that the addition of the functional silane slightly accelerated both the growth and structural deformation of the materials. The results were discussed based on the kinetics of the cooperative assembly of silicate species and the micelles of mixed surfactants and the interplay between the hydrolyzed silanes and surfactant molecules.
© 2011 Elsevier Inc. All rights reserved.

1. Introduction

Ordered mesoporous silica-based materials are attractive for the construction of advanced materials on the nanometer scale. The ability to control their structural and textural properties and to functionalize them with organic groups and/or inorganic entities holds the key to their promising applications [1–11]. Surfactant-templated mesoporous silica materials generally exhibit pore topologies correlated to those observed for the liquid–crystal phases of surfactant-water systems [2,6,12,13]. MCM-41 with two-dimensional (2D)-hexagonal (plane group *p6mm*) structure is the most well known example [14,15]. Between 2D-hexagonal and lamellar phases, there exist so-called ribbon phases that consist of noncircular micellar rods arranged on a 2D-rectangular lattice [16–18]. Ribbon phases and can be regarded as deformed phases of the 2D-hexagonal phase, and mesostructured silica materials correlated to the ribbon phases are rare. Examples include SBA-8 and M_α silicas with centered-rectangular (plane group *c2mm*) mesostructures synthesized by using bolaform and gemini surfactants [19] and a primitive-rectangular (plane group *p2gg*) silica mesophase identified as an intermediate phase between 2D-hexagonal chiral and lamellar mesostructures [20]. The ribbon-phase-correlated mesoporous silica materials are unique and interesting owing to their low-symmetry and deformed mesostructure.

On the other hand, mesoporous silica materials can be organically functionalized by post-synthesis grafting or via cocondensation synthesis [4,8]. The cocondensation of tetraalkoxysilanes and terminal or bridged organosilanes in the presence of structure-directing surfactants leads to materials with organic groups that are covalently anchored and usually distributed homogeneously on or in the pore walls. The method has been applied to synthesize functionalized materials having helical [21–23] or other morphologies [4,8,11]. A problem often encountered for cocondensation is the decreased structural order owing to the interference of organosilane in the cooperative assembly of surfactant molecules and silicate species [4,8]. Nevertheless, it has been observed, in only a few cocondensation systems, that changing the amount of organosilane could induce structural transformation between ordered mesophases [24–31]. Therefore, not only being a method of functionalization, the cocondensation synthesis could also be a versatile way for structural modulation.

Recently, we discovered a new type of mesoporous silica materials with 2D-rectangular *c2mm* symmetry and helical morphology [32,33]. The materials, designated as MMT-1, were synthesized in the dilute solution of mixed surfactants of cetyltrimethylammonium bromide (CTAB) and tetraethylene glycol dodecyl ether ($C_{12}EO_4$) [32]. In this work, we report the first cocondensation synthesis of functionalized MMT-1 materials with *c2mm* mesostructure

* Corresponding author at: Department of Chemistry, National Tsing Hua University, Hsinchu 30013, Taiwan. Tel.: +886 3 5731282; fax: +886 3 5165521.
E-mail address: cmyang@mx.nthu.edu.tw (C.-M. Yang).

1387-1811/$ - see front matter © 2011 Elsevier Inc. All rights reserved.
doi:10.1016/j.micromeso.2011.09.033

and helical channel-type mesopores. The thiol (mercaptopropyl) functionality was chosen because of its promising applications for selective ion adsorption [34], protein immobilization [35], controlled growth of gold nanoparticles [23,36], and the preparation of sulfonic solid acids [37,38]. Ordered mercaptopropyl-functionalized helical MMT-1 nanoparticles were successfully synthesized by the cocondensation with 3-mercaptopropyltrimethoxysilane (MPTMS) in the mixed CTAB/$C_{12}EO_4$ solution. Interestingly, we found that an increase of the amount of MPTMS resulted in a decrease of structural anisotropy and a *c2mm*-to-*p6mm* structural transformation, and that a reverse *p6mm*-to-*c2mm* transformation took place when the percentage of $C_{12}EO_4$ in the surfactant mixture was further increased. Moreover, we found that the presence of $C_{12}EO_4$ is essential for forming the short-pitch helical channels in the functionalized materials. *In situ* small-angle X-ray scattering (SAXS) measurements were also performed to study the structural evolution during the cocondensation synthesis. The results are discussed based on the kinetics of the cooperative assembly of silicate species and the micelles of mixed CTAB/$C_{12}EO_4$ and the interplay between the hydrolyzed MPTMS and surfactant molecules.

2. Experimental section

Synthesis. Mercaptopropyl-functionalized materials were synthesized by injecting a mixture of tetraethoxysilane (TEOS, ACROS) and MPTMS (Gelest) into the alkaline solution of CTAB (ACROS) and $C_{12}EO_4$ (Aldrich) at a rate of 7.5 mL h^{-1} with sodium hydroxide as a base. The mixture was stirred at 308 K for 2 h followed by aging at 363 K for one day. The product was filtered, washed with acetone and finally dried in air. The molar composition of the synthesis mixture was $(1-x\%)$TEOS:$x\%$MPTMS:$0.125\times(1-y\%)$CTAB:$0.125\times(y\%)C_{12}EO_4$:0.3NaOH:1230$H_2O$, where $x\%$ is the mole percentage of MPTMS in the silane mixture ($0<x<10$) and $y\%$ is the mole percentage of $C_{12}EO_4$ in the surfactant mixture ($25<y<45$). The resulting samples are referred to as SHx-fy. The mole percentage of $C_{12}EO_4$ for most syntheses was 25% to produce materials with the highest structural order [32]. The surfactants in the as-synthesized samples were removed by extraction in a hydrochloric acid–ethanol mixture.

Selected samples were applied to adsorb chloroauric ions for the deposition of gold nanoparticles. A surfactant-free sample (0.1 g) was added and stirred in the aqueous solution of chloroauric acid (25 mM, 5 mL) at room temperature for 20 min. The sample was filtered and washed repeatedly with copious amounts of water to remove un-adsorbed chloroauric ions. The metal in the dried sample was reduced in a hydrogen flow at 423 K.

Characterization. X-ray diffraction (XRD) patterns were recorded on a Mac Science 18MPX diffractometer using Cu Kα radiation. Solid-state ^{29}Si MAS NMR spectra were measured on a Bruker DSX400WB spectrometer using a 7-mm probe. Nitrogen physisorption isotherms were measured at 77 K using a Quantachrome Autosorb-1MP instrument. The isotherms were analyzed by nonlocal density functional theory (NLDFT) (by applying a N_2 (77 K) kernel based on cylindrical pore geometry) to evaluate the pore size and surface area of the samples. The total pore volume was evaluated at a relative pressure (P/P_0) of 0.85. Scanning electron microscopy (SEM) images were obtained with a field emission JEOL JSM-7000F microscope operating at 10 kV. The samples were coated with Pt before measurements. Transmission electron microscopy (TEM) images were taken using a JEOL JEM-2010 microscope operated at 200 kV. Energy dispersive X-ray (EDX) spectroscopy was applied using an Oxford EDX system.

In situ SAXS measurements were performed at the beamline 17B3 of the National Synchrotron Radiation Research Center (NSRRC), Taiwan, using X-ray with a photon energy of 10.0 keV. One-dimensional SAXS profiles were circularly averaged from 2D images obtained using a multiwire area detector (gas-type). The sample-to-detector distance was 1751.72 mm. The scattering wavevector q, $4\pi\sin(\theta)/\lambda$, defined by the scattering angle 2θ and wavelength λ, was calibrated with silver behenate, and the scattering intensity $I(q)$ was calibrated to the absolute intensity scale with a polyethylene sample. Each reaction for the measurement was carried out in a batch reactor, and the silica source was injected with a controlled rate to the reaction mixture using a syringe pump. The reaction mixture was continuously pumped through a Kapton-sealed thin container, through which the X-ray beam passed, and then back to the reactor at a pumping rate of

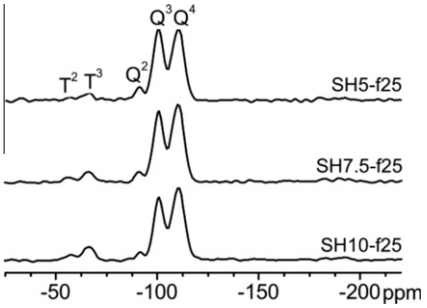

Fig. 1. ^{29}Si MAS NMR spectra of selected mercaptopropyl-functionalized samples.

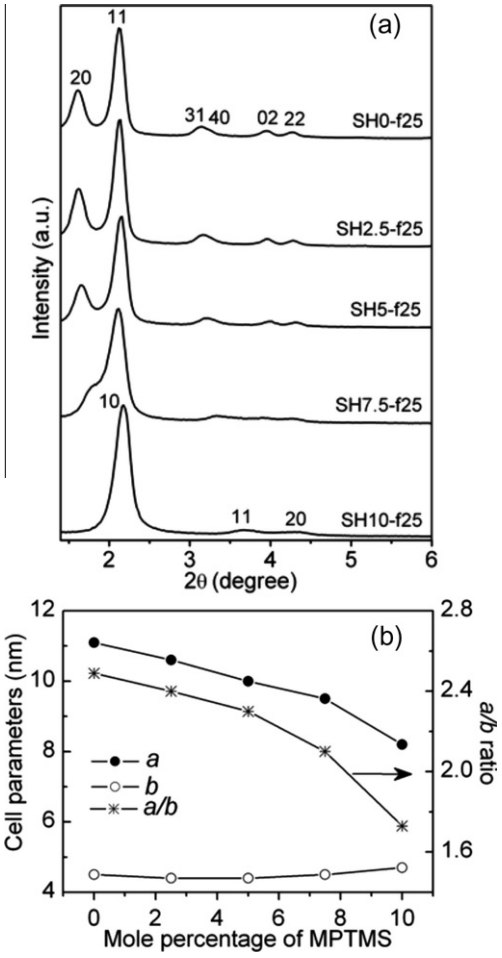

Fig. 2. (a) XRD patterns of SHx-f25 samples and (b) the calculated cell parameters *a* and *b* and their ratio.

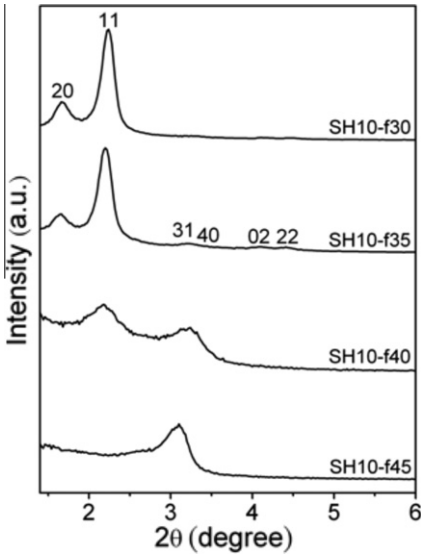

Fig. 3. XRD patterns of SH10-fy samples.

40 mL min^{-1}. Both the reactor and the container were thermostated to a desired temperature of 308 K.

3. Results and discussion

The incorporation of mercaptopropyl groups in the materials was studied by ^{29}Si MAS NMR, and Fig. 1 shows the spectra of SHx-f25 samples synthesized with x = 5.0, 7.5 and 10.0. The spectra exhibit lines attributed to T^n groups ($Si(OSi)_n(OH)_{3-n}C$) stemming from the silicon of functional silane and lines attributed to Q^n groups ($Si(OSi)_n(OH)_{4-n}$) stemming from the silicon of silica backbone. The $T/T+Q$ ratios of the integral intensities of the lines of the two groups are 0.06, 0.08 and 0.11, respectively. The values match the corresponding mole percentages of MPTMS in the silane mixtures, suggesting that nearly all the MPTMS molecules were incorporated into the samples during cocondensation synthesis.

The addition of MPTMS affected the mesostructure of resulting materials. Fig. 2(a) shows the XRD patterns of the surfactant-free SHx-f25 samples. The pure-silica sample (SH0-f25) exhibits well-resolved peaks attributed to 20, 11 and other high-order reflections of a 2D-rectangular *c2mm* structure [32]. For the mercaptopropyl-functionalized samples, with increasing x from 2.5 to 7.5, 20

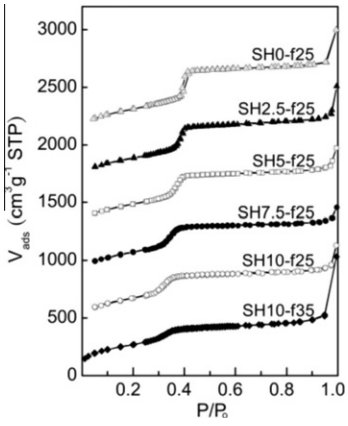

Fig. 4. Nitrogen physisorption isotherms (at 77 K) for the selected samples. The isotherms (from bottom to top) are shifted by 0, 400, 800, 1200, 1600 and 2000 cm^3 g^{-1} STP, respectively.

Table 1
Textural data of the selected samples.[a]

Sample	S [m^{2}g^{-1}]	V [cm^{3}g^{-1}]	D [nm]
SH0-f25	1120	0.97	4.2
SH2.5-f25	1035	0.90	4.0
SH5-f25	1023	0.87	4.0
SH7.5-f25	996	0.81	3.9
SH10-f25	937	0.78	3.7
SH10-f35	897	0.74	3.7

[a] S: surface area; V: total pore volume; D: mean pore diameter.

reflection shifts toward higher angle while the position of 11 reflection remains relatively unchanged. Other high-order reflections slightly shift correspondingly and all the patterns could still be indexed with a *c2mm* lattice. It indicates that, as shown in Fig. 2(b), the cell parameter a is decreased from 11.1 to 9.5 nm as increasing x from 0 to 7.5 whereas the parameter b remains roughly unchanged (4.4–4.5 nm). As a consequence, the a/b ratio

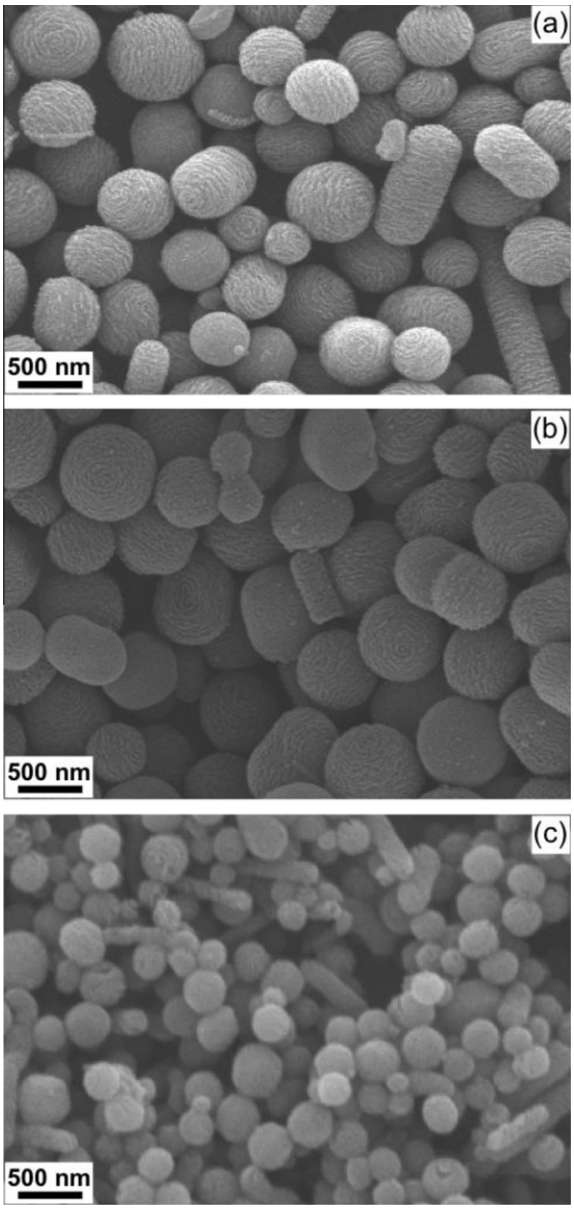

Fig. 5. SEM images of (a) SH5-f25, (b) SH10-f25, and (c) SH10-f35.

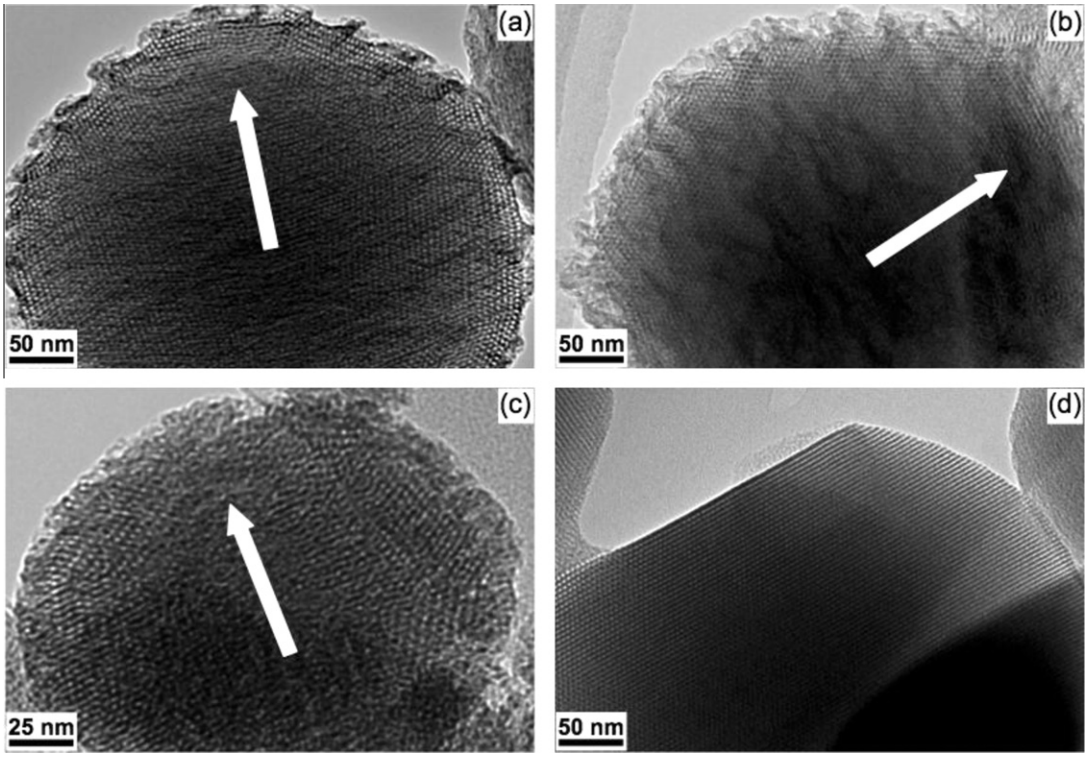

Fig. 6. TEM images of (a) SH5-f25, (b) SH10-f25, (c) SH10-f35, and (d) SH10-f0.

decreases from 2.49 for $x = 0$ to 2.10 for $x = 7.5$. For SH10-f25, its XRD pattern can be perfectly indexed with a *p6mm* lattice ($d_{10}/d_{11} = \sqrt{3}$, $d_{10}/d_{20} = 2$, $a/b = 1.73 - \sqrt{3}$). Clearly, the addition of MPTMS in cocondensation synthesis led to a decrease of the anisotropy of the *c2mm* mesostructure (*i.e.* the deviation of the a/b ratio from $\sqrt{3}$) and a *c2mm*-to-*p6mm* structural transformation.

Interestingly, the transformation could be reversed by further increasing the mole percentage (y) of $C_{12}EO_4$. As shown in Fig. 3, a slight change of y from 25 to 30 already gave a sample (SH10-f30) exhibiting a XRD pattern indicative of a *c2mm* mesostructure with an a/b ratio of 2.44 (a = 10.5 nm and b = 4.3 nm). The structure remained for the sample with $y = 35$, but adding too much $C_{12}EO_4$ ($y \geq 40$) resulted in materials with disordered structure (cf. the XRD patterns of SH10-f40 and SH10-f45 in Fig. 3). It seems that adding more $C_{12}EO_4$ may counteract the influence of MPTMS on the formation of ordered materials in the dilute and alkaline solution of mixed CTAB/$C_{12}EO_4$. In addition, compared to other condensation systems showing organosilane-induced structural transformations [24–31], the synthesis system under study is unique because of the flexibility to modulate the 2D-rectangular lattice of the functional mesostructures.

The textural characteristics of the surfactant-free materials with different amount of mercaptopropyl groups (i.e. SHx-f25 and SH10-f35) were analyzed by nitrogen physisorption measurements. As shown in Fig. 4(a), all the isotherms are type IV curves exhibiting steps over the relative pressure range of 0.25–0.4. For SHx-f25 samples, the step becomes smaller and wider and shifts toward smaller relative pressure with increasing x from 0 to 10, suggesting smaller pore volume, wider pore size distribution and smaller mean pore diameter for the samples with higher loadings of mercaptopropyl groups. The textural data are listed in Table 1. The isotherms for all the samples except SH0-f25 do not show any hysteresis loops because at 77 K the pore fluid in the channels with a mean diameter smaller than 4 nm is above so-called hysteresis critical temperature [39]. SH0-f25 has a mean pore diameter of 4.2 nm and it gave an isotherm exhibiting a very narrow loop. The textural properties are related to the shape (or the ellipticity) of channels in the *c2mm* mesostructure [32,33] and the presence of mercaptopropyl groups on the mesopore surface, and the latter seems to have stronger influence since all the textural properties change monotonically with an increase of the amount of the functional groups. It could also explain why the isotherm of SH10-f35 (with a *c2mm* structure and a a/b ratio of 2.44) is similar to the isotherm of SH10-f25 (with a *p6mm* structure) rather than to that of SH2.5-f25 with a similar *c2mm* lattice (a/b = 2.40).

Despite having distinct mesostructures, SEM and TEM studies revealed similar morphology and pore arrangement for the ordered mercaptopropyl-functionalized materials. Fig. 5 shows the SEM images of the selected samples with *c2mm* or *p6mm* symmetry. All the samples are mainly composed of spherical nanoparticles, with some elongated rod-like particles as minor products. Furthermore, the observed circling stripes on the surface of all the particles imply a short-pitch helical pore arrangement for these materials. Indeed, the TEM images in Fig. 6 reveal that, just like the pure-silica helical mesoporous materials with short (just a few lattice constants) helical pitch [32,33,40,41], the channel-type mesopores in these materials are coiled around a center axis (indicated by the arrow) and the shape of channel section can be clearly seen at both sides of the particles. The elliptical channels in SH5-f25 are arranged in a 2D-rectangular symmetry, while the cylindrical channels in SH10-f25 are packed into a 2D-hexagonal structure. The nanoparticles in SH10-f35 are smaller than those in other SHx-f25 samples but they also have helical and elliptical channels. The nonionic surfactant $C_{12}EO_4$ seems to be associated with helical arrangement of the channels in these materials since the CTAB-templated mercaptopropyl-functionalized MCM-41 materials synthesized by cocondensation were reported to have straight and cylindrical mesopores [42]. To verify it, a $C_{12}EO_4$-free ($y = 0$) cocondensation synthesis with a molar percentage of MPTMS of 10% ($x = 10$) was performed, and the TEM image of the

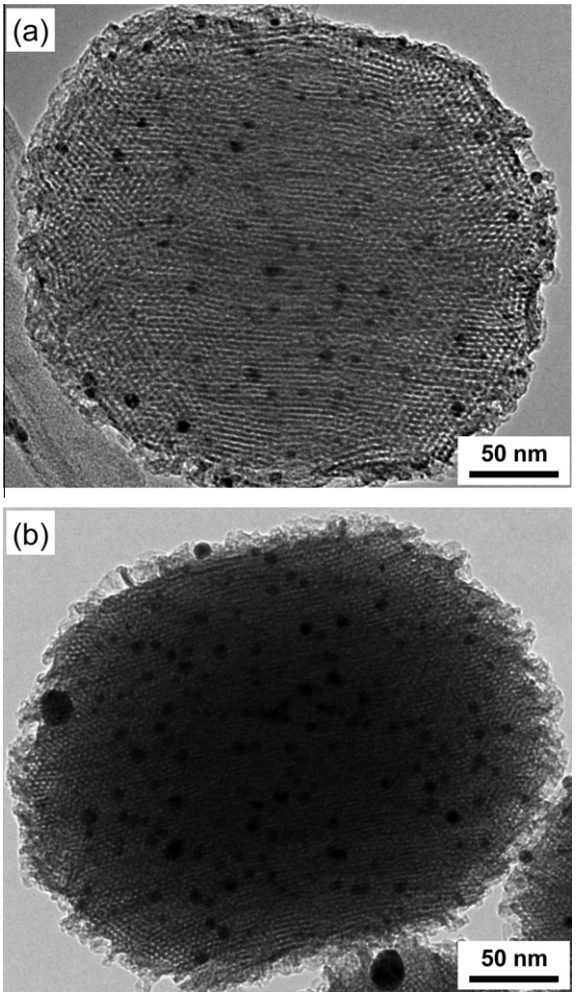

Fig. 7. TEM images of the Au@SH5-f25 and Au@SH10-f25 composites.

resulting sample SH10-f0 (with *p6mm* symmetry) clearly shows straight channels in rod-like particles (cf. Fig. 6(d)). The results confirm the crucial role of $C_{12}EO_4$ in forming helical channels in the materials with either *c2mm* or *p6mm* symmetry.

The distribution of mercaptopropyl groups in the functional materials was also studied. EDX spectroscopy was applied to all the samples investigated by TEM, and around 20 nanoparticles (including rod-like minor products) in each sample were individually analyzed. The sulfur-to-silicon (S/Si) atomic ratios were almost identical for all the nanoparticles in each sample, and the average values of S/Si ratio were consistent with the results of ^{29}Si MAS NMR for all the samples investigated. Moreover, selected samples were deposited with gold nanoparticles by reducing chloroauric ions selectively adsorbed on mercaptopropyl groups. The TEM images of Au@SH5-f25 and Au@SH10-f25 composites in Fig. 7 show that Au nanoparticles with sizes of 2–4 nm are uniformly distributed in the two samples, suggesting that the mercaptopropyl groups are homogeneously anchored on the surface of channels.

The structural evolution during cocondensation synthesis of SH2.5-f25, SH5-f25 and SH10-f25 was also studied by *in situ* SAXS and the data are shown in Fig. 8. For the synthesis of SH2.5-f25 and SH5-f25, ordered mesophases were formed at around 18 min after adding TEOS/MPTMS mixture and a Bragg peak at $q = 0.134$ Å^{-1} (corresponding to a *d*-spacing (*d*) of 4.7 nm) appeared in the SAXS patterns. The peak quickly split into two peaks that further evolved and moved away from each other and became more intense. Other high-order Bragg peaks appeared at a reaction time (*t*) of about 24 min. All the peaks could be indexed assuming a 2D-rectangular *c2mm* lattice and the derived values of unit cell parameters *a* and *b* are shown in the insets of the figures. The *a*/*b* ratios at $t = 26$ min were 2.39 and 2.32 for SH2.5-f25 and SH5-f25, respectively, and the values remained unchanged since then. Compared to the formation of pure-silica MMT-1 materials synthesized using TEOS as a silica source [32,33], the structural transformation for the mercaptopropyl-functionalized samples was completed within a shorter period of time (~6 min), but the degree of structural transformation was smaller. Moreover, the change of the intensity of 11 Bragg peak was analyzed by applying the Avrami–Erofe'ev expression [43–46] to derive the rate constant for materials growth. The rate constants are 8.8×10^{-4} s^{-1} and 9.0×10^{-4} s^{-1} for SH2.5-f25 and SH5-f25, respectively, slightly larger than that (8.0×10^{-4} s^{-1}) for pure-silica MMT-1 (i.e. SH0-f25) [33]. For SH10-f25, the induction

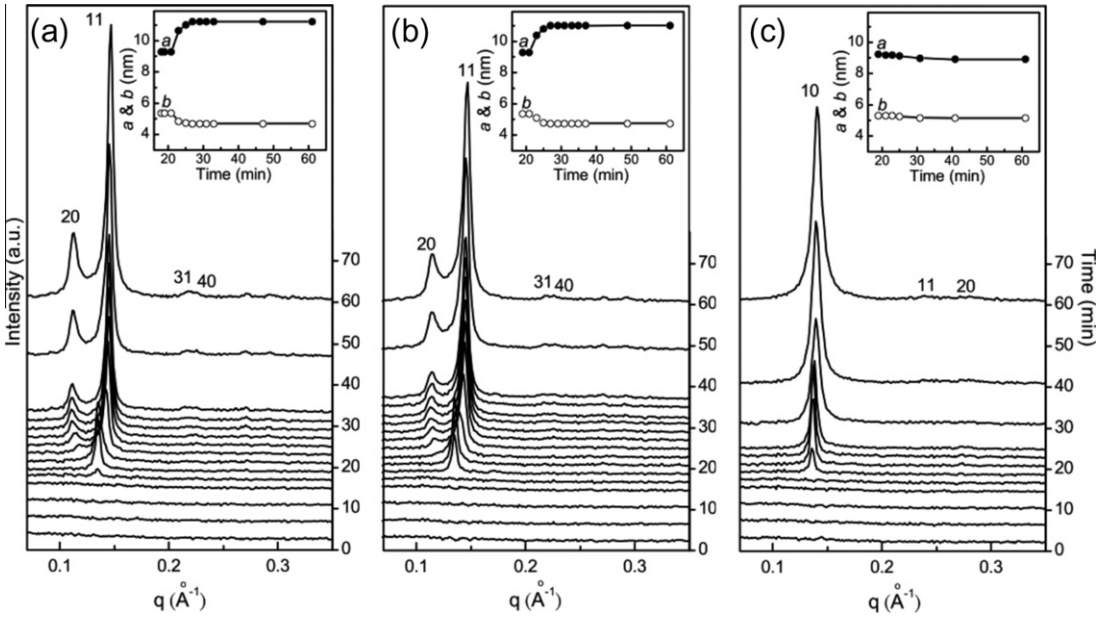

Fig. 8. *In situ* SAXS data for the cocondensation syntheses of (a) SH2.5-f25, (b) SH5-f25, and (c) SH10-f25. The insets are the temporal evolution of the cell parameters *a* and *b*.

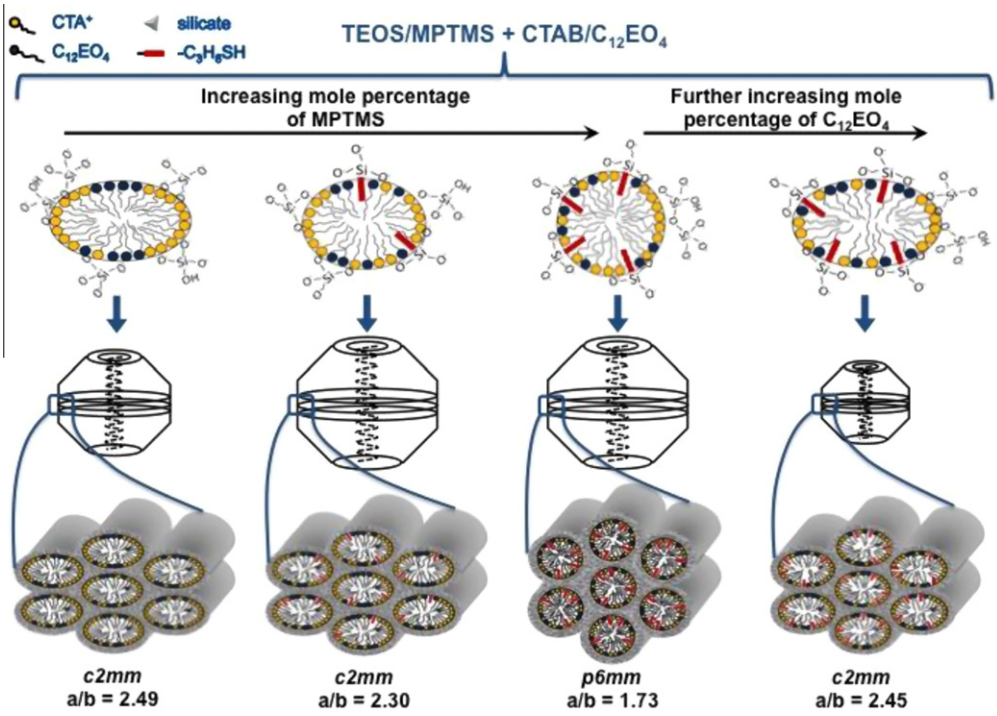

Fig. 9. Schematic representation of the formation of the mercaptopropyl-functionalized materials synthesized with different mole percentages of MPTMS and $C_{12}EO_4$ in the dilute solution of mixed CTAB/$C_{12}EO_4$.

time (~18 min) for forming *p6mm* mesostructure and the rate constant for materials growth (9.1×10^{-4} s^{-1}) are almost identical to those for SH2.5-f25 and SH5-f25. The results suggest that the addition of MPTMS slightly accelerates the formation of ordered functional materials regardless of the symmetry of mesostructures.

The cocondensation synthesis of the mercaptopropyl-functionalized nanoparticles in dilute and alkaline solution of mixed CTAB/$C_{12}EO_4$ is unique because the resulting materials have adjustable 2D-rectangular lattice and short-pitch helical arrangement of channels. The formation of these functional nanomaterials should be related to cooperative assembly of silicate species and the micelles of mixed surfactants and the interplay between the hydrolyzed MPTMS and surfactant molecules. As shown in Fig. 9, upon being added into the synthesis solution, TEOS (and MPTMS) readily hydrolyzes to form anionic silicate species that diffuse and preferentially adsorb onto cetyltrimethylammonium (CTA) cations in the micelles [2]. For the formation of pure-silica MMT-1 with a mole percentage of $C_{12}EO_4$ of 25% (i.e. SH0-f25), further hydrolytic condensation of silicates would then pull CTA cations together, induce a segregation of the two surfactants, and result in a deformed and elliptical micellar rods with $C_{12}EO_4$ enriched at the less curved parts due to a much weaker repulsion between nonionic head groups of $C_{12}EO_4$ [32,33]. In the mean time, the silicate-encased micellar rods continue to fuse and elongate, bend and coil due to further silicate condensation at the CTA-enriched (highly curved) parts of the rods, and pack into a 2D-rectangular *c2mm* mesostructure. Concerning the cocondensation synthesis with MPTMS, since the pH value (~9.8) of synthesis solution is lower than the pK_a (~10.5) of mercaptopropyl group, most of the groups are neutral and less polar and the mercaptopropylsilyl anions from the hydrolyzed MPTMS may be intercalated in the micelles. The intercalated mercaptopropylsilyl anions may facilitate the interfacial condensation of silicate species and slightly speed up structural transformation and the growth of mesostructure, as observed by *in situ* SAXS. They may also reduce charge density of the head groups of CTA cations, thereby retarding surfactants segregation, decreasing the curvature at the CTA-enriched portion of micelles, and reducing the degree of deformation of mesostructure (as compared to a 2D-hexagonal *p6mm* mesostructure with cylindrical micellar rods). The more MPTMS is added (and therefore more mercaptopropylsilyl groups are intercalated in the micelles), the less the degree of structural deformation would be. With a MPTMS mole percentage of 10%, the sample (i.e. SH10-f25) exhibits a 2D-hexagonal *p6mm* mesostructure. The mesostructure could be deformed again to *c2mm* mesophase by further increasing the mole percentage of $C_{12}EO_4$ to 25–35%, because additional $C_{12}EO_4$ molecules would again form segregated and flattened domains in the deformed micelles. Finally, the key role of $C_{12}EO_4$ in forming helical micellar rods (or helical channel arrangement) in the final samples could be also realized by recognizing the differential rates of silicate condensation nearby $C_{12}EO_4$ and CTA cations that would subsequently make the elongated micellar rods bend and coiled into a helical mesostructure, a process mainly driven by a reduction in surface free energy [21,32,33,47].

4. Conclusions

Mercaptopropyl-functionalized mesoporous silica nanoparticles with *c2mm* symmetry and short-pitch helical channels have been prepared by cocondensation synthesis in dilute and alkaline solution of mixed CTAB/$C_{12}EO_4$. The 2D-rectangular lattice of the materials can be modulated by adjusting relative amounts of MPTMS or $C_{12}EO_4$, and the helical arrangement of channels is related to the presence of $C_{12}EO_4$. The textural properties of the materials are mainly affected by the amount of mercaptopropyl groups that are uniformly distributed on the surface of channels. The addition of MPTMS slightly accelerates materials growth as well as structural deformation to result in final ordered mesophases. The observed phenomena have been discussed based on the assembly kinetics involving MPTMS and mixed surfactants.

Acknowledgements

The authors thank U.S. Jeng, Y.H. Lai and C.H. Su (NSRRC) for their help with SAXS measurements. The authors also thank National Tsing Hua University and the National Science Council of the Republic of China for financial support under the contract no. NSC98-2113-M-007-020-MY3.

References

[1] K. Moller, T. Bein, Chem. Mater. 10 (1998) 2950.
[2] U. Ciesla, F. Schüth, Micropor. Mesopor. Mater. 27 (1999) 131.
[3] J.Y. Ying, C.P. Mehnert, M.S. Wong, Angew. Chem.-Int. Edit. 38 (1999) 56.
[4] A. Stein, B.J. Melde, R.C. Schroden, Adv. Mater. 12 (2000) 1403.
[5] F. Schüth, W. Schmidt, Adv. Mater. 14 (2002) 629.
[6] G.J.D. Soler-illia, C. Sanchez, B. Lebeau, J. Patarin, Chem. Rev. 102 (2002) 4093.
[7] C.M. Yang, K.J.J. Chao, Chin. Chem. Soc. 49 (2002) 883.
[8] F. Hoffmann, M. Cornelius, J. Morell, M. Froba, Angew. Chem.-Int. Edit. 45 (2006) 3216.
[9] Y. Wan, Y.F. Shi, D.Y. Zhao, Chem. Commun. (2007) 897.
[10] I.I. Slowing, B.G. Trewyn, S. Giri, V.S.Y. Lin, Adv. Funct. Mater. 17 (2007) 1225.
[11] B.G. Trewyn, I.I. Slowing, S. Giri, H.T. Chen, V.S.Y. Lin, Acc. Chem. Res. 40 (2007) 846.
[12] Q.S. Huo, D.I. Margolese, U. Ciesla, P.Y. Feng, T.E. Gier, P. Sieger, R. Leon, P.M. Petroff, F. Schuth, G.D. Stucky, Nature 368 (1994) 317.
[13] S. Che, A.E. Garcia-Bennett, T. Yokoi, K. Sakamoto, H. Kunieda, O. Terasaki, T. Tatsumi, Nat. Mater. 2 (2003) 801.
[14] C.T. Kresge, M.E. Leonowicz, W.J. Roth, J.C. Vartuli, J.S. Beck, Nature 359 (1992) 710.
[15] J.S. Beck, J.C. Vartuli, W.J. Roth, M.E. Leonowicz, C.T. Kresge, K.D. Schmitt, C.T.W. Chu, D.H. Olson, E.W. Sheppard, S.B. McCullen, J.B. Higgins, J.L.J. Schlenker, Am. Chem. Soc. 114 (1992) 10834.
[16] F. Husson, H. Mustacchi, V. Luzzati, Acta Crystallogr. 13 (1960) 668.
[17] H. Hagslatt, O. Soderman, B. Jonsson, Liq. Cryst. 12 (1992) 667.
[18] S. Gustafsson, P.O. Quist, B. Halle, Liq. Cryst. 18 (1995) 545.
[19] D.Y. Zhao, Q.S. Huo, J.L. Feng, J.M. Kim, Y.J. Han, G.D. Stucky, Chem. Mater. 11 (1999) 2668.
[20] H.B. Qiu, Y. Sakamoto, O. Terasaki, S.N. Che, Adv. Mater. 20 (2008) 425.
[21] L. Zhang, S.Z. Qiao, Y.G. Jin, L.N. Cheng, Z.F. Yan, G.Q. Lu, Adv. Funct. Mater. 18 (2008) 3834.
[22] H.M. Chen, J.H. He, Dalton Trans. (2009) 6651.
[23] F. Rambaud, K. Valle, S. Thibaud, B. Julian-Lopez, C. Sanchez, Adv. Funct. Mater. 19 (2009) 2896.
[24] Y.Q. Wang, C.M. Yang, B. Zibrowius, B. Spliethoff, M. Linden, F. Schuth, Chem. Mater. 15 (2003) 5029.
[25] R.P. Hodgkins, A.E. Garcia-Bennett, P.A. Wright, Micropor. Mesopor. Mater. 79 (2005) 241.
[26] Y.Q. Wang, Y.J. Wang, C.M. Yang, G.Z. Lu, F. Schuth, Langmuir 22 (2006) 5491.
[27] R.M. Grudzien, S. Pikns, M.J. Jaroniec, Phys. Chem. C 113 (2009) 4875.
[28] C.B. Gao, Y. Sakamoto, O. Terasaki, S.A. Che, Chem.-Eur. J. 14 (2008) 11423.
[29] H.I. Lee, C. Pak, S.H. Yi, J.K. Shon, S.S. Kim, B.G. So, H. Chang, J.E. Yie, Y.U. Kwon, J.M.J. Kim, Mater. Chem. 15 (2005) 4711.
[30] L. Han, Y. Sakamoto, O. Terasaki, Y. Li, S.J. Che, Mater. Chem. 17 (2007) 1216.
[31] R. Atluri, Y. Sakamoto, A.E. Garcia-Bennettt, Langmuir 25 (2009) 3189.
[32] C.M. Yang, C.Y. Lin, Y. Sakamoto, W.C. Huang, L.L. Chang, Chem. Commun. (2008) 5969.
[33] W.C. Huang, L.L. Chang, Y. Sakamoto, C.Y. Lin, N.C. Lai, C.M. Yang, RSC Advances, 2011.
[34] X. Feng, G.E. Fryxell, L.Q. Wang, A.Y. Kim, J. Liu, K.M. Kemner, Science 276 (1997) 923.
[35] H.H.P. Yiu, C.H. Botting, N.P. Botting, P.A. Wright, PCCP 3 (2001) 2983.
[36] Y. Guari, C. Theiuleux, A. Mehdi, C. Reye, R.J.P. Corriu, S. Gomez-Gallardo, K. Philippot, B. Chaudret, R. Dutartre, Chem. Commun. (2001) 1374.
[37] M.H. Lim, C.F. Blanford, A. Stein, Chem. Mater. 10 (1998) 467.
[38] W.M. Van Rhijn, D.E. De Vos, B.F. Sels, W.D. Bossaert, P.A. Jacobs, Chem. Commun. (1998) 317.
[39] S. Lowell, J.E. Shields, M.A. Thomas, M. Thommes, Characterization of Porous Solids and Powders: Surface Area, Pore size and Density, 2004.
[40] Q.S. Huo, D.Y. Zhao, J.L. Feng, K. Weston, S.K. Buratto, G.D. Stucky, S. Schacht, F. Schuth, Adv. Mater. 9 (1997) 974.
[41] F. Marlow, B. Spliethoff, B. Tesche, D.Y. Zhao, Adv. Mater. 12 (2000) 961.
[42] M.J. Avrami, Chem. Phys. 7 (1939) 1103.
[43] M.J. Avrami, Chem. Phys. 8 (1940) 212.
[44] M.J. Avrami, Chem. Phys. 9 (1941) 177.
[45] B.V.C.R. Erofe'ev, Dokl. Acad. Sci. URSS 52 (1946) 511.
[46] S. Yang, L.Z. Zhao, C.Z. Yu, X.F. Zhou, J.W. Tang, P. Yuan, D.Y. Chen, D.Y.J. Zhao, Am. Chem. Soc. 128 (2006) 10460.